Analytical Methods

ROYAL SOCIETY OF CHEMISTRY

PAPER

View Article Online
View Journal | View Issue

Cite this: *Anal. Methods*, 2020, **12**, 5671

A hybrid electronic nose system for discrimination of pathogenic bacterial volatile compounds

Thara Seesaard, [a] Chadinee Thippakorn, [b] Teerakiat Kerdcharoen[c] and Sumana Kladsomboon *[d]

A hybrid electronic nose comprising an array of three organic–inorganic nanocomposite gas sensors [zinc tetra *tert*-butyl phthalocyanine (ZnTTBPc), zinc tetra-phenyl porphyrin (ZnTPP), and cobalt tetraphenyl-porphyrin (CoTPP)] coupled with three commercial metal-oxide semiconductor gas sensors (TGS 2444, TGS 2603 and TGS 2620) was developed to discriminate bacterial volatile compounds. Each type of gas sensor had its own strengths and weaknesses in terms of its capability to detect complex odors from the five different bacterial species tested. Bacterial samples were controlled at a fixed initial bacterial concentration by measuring the optical density at 600 nm of the culture suspensions. A comparative evaluation of the volatile compound fingerprints from five bacterial species grown in Luria–Bertani medium was conducted to identify the optimal incubation time for detection of volatile biomarkers to discriminate among bacteria. The results suggest that the hybrid electronic nose was indeed able to discriminate among the bacterial species and culture media, with a variance based on contributions of 92.4% from PC1 and 7.2% from PC2, at an incubation time of 6 hours. Furthermore, the results of hierarchical cluster analysis showed that bacterial odor data formed two major bacterial groups, with the maximum cluster distance close to 25. Intra-group similarity was demonstrated as the two bacterial species (*E. cloacae* and *P. aeruginosa*) from among the Gram-negative bacteria had a greater similarity with a cluster distance close to 4. Finally, the minimum distance between *E. cloacae* and *S.* Typhi was approximately 1, at an equal distance from *E. coli* and *S. aureus*.

Received 29th June 2020
Accepted 6th November 2020

DOI: 10.1039/d0ay01255f

rsc.li/methods

1. Introduction

Bacterial infection is one of the most important human health problems. It can not only happen more often in people with pre-existing illnesses, but can also occur in a healthy person. Most species of pathogenic bacteria are found as contaminants in the environment, such as in recreational water,[1] slum areas[2] and industrial lands.[3] Bacterial pathogens are often spread through urine and feces. They may infect the skin and underlying soft tissue, as does *Staphylococcus aureus*.[4] There are several types of Gram-negative pathogenic bacteria, including *Pseudomonas aeruginosa* (*P. aeruginosa*), *Escherichia coli* (*E. coli*), *Enterobacter cloacae* (*E. cloacae*) and *Salmonella* Typhi (*S.* Typhi). For example, *P. aeruginosa* can cause opportunistic human infections such as septicemia and pneumonia,[5] and *E. coli* can cause serious food poisoning or toxicity.[6] *E. cloacae* can cause urinary tract infection or pneumonia,[7] while *S.* Typhi causes gastrointestinal infection.[8]

The rapid and accurate identification of the cause of an illness is considered the heart of disease diagnosis. The detection of pathogenic organisms allows intervention to prevent or limit tissue invasion. The precise identification of bacterial species is extremely important in patients because it guides to the most appropriate treatment. Many researchers have tried to develop methods for the early detection of pathogenic bacteria.[9] Using traditional approaches, the identification of bacterial species takes an average of 16–72 hours with techniques such as bacterial culturing,[8] molecular methods,[10] microscopic observation[11] and biochemical testing.[12] Microbiological culturing is one of the primary diagnostic methods in microbiology.[12] Bacterial culturing of body fluids from patients and from environmental specimens remains the gold standard in the diagnosis of most bacterial infections.[13] A revolutionary method, matrix-assisted laser desorption/ionization-time of flight mass spectrometry (MALDI-TOF MS)[14] provides the rapid identification of bacteria and is now popular in advanced clinical laboratories. However, some of these identification methods have not been entirely successful for some bacterial strains. Furthermore, in some remote areas acquiring expensive

[a]*Department of Physics, Faculty of Science and Technology, Kanchanaburi Rajabhat University, Kanchanaburi, 71190, Thailand*

[b]*Center for Research and Innovation, Faculty of Medical Technology, Mahidol University, Phutthamonthon, Nakhon Pathom, 73170, Thailand*

[c]*Department of Physics, Faculty of Science, Mahidol University, Bangkok, 10400, Thailand*

[d]*Department of Radiological Technology, Faculty of Medical Technology, Mahidol University, Phutthamonthon, Nakhon Pathom, 73170, Thailand. E-mail: sumana.kla@mahidol.edu; Tel: +66-89-119-4147*

equipment is not possible. But for laboratories conducting high-throughput detection (*e.g.*, a daily analysis of at least 100 strains), it can be considered a very cost-effective investment.

The development of one alternative method to identify bacterial species has been conducted based on detection of bacterial volatile organic compounds (VOCs).[15] In recent decades, the application of the gas chromatography-mass spectrometry (GC-MS) technique combined with special statistical approaches has been proposed to identify specific bacterial VOC profiles.[16] As summarized in Table 1, many studies have found that there are seven groups of VOCs that are released during bacterial growth, namely, volatile sulfur compounds (VSCs), aldehydes, acids, ketones, hydrocarbons, alcohols and volatile nitrogen compounds (VNCs).[17,18] These growth stage-specific volatile compounds have profiles which are distinct for different species of bacteria. For example, VSCs, aldehydes, acids, ketones, hydrocarbons, alcohols and VNCs are normally produced by *P. aeruginosa*, while ketones and alcohols are observed with *E. cloacae*.[16,19,20] Thus, four species of Gram-negative bacteria and one species of Gram-positive bacteria can produce unique VOC profiles (see Table 1). Although the GC/MS technique is a non-invasive diagnostic tool, the method is complex and the hardware is expensive.[21] Thus, the development of bacterial identification tools, which are accurate, rapid, easy to use and cost-effective, is very challenging.

In recent decades, researchers have revealed that an electronic nose is considered to be a non-invasive tool to assess bacterial volatile compounds using gas sensor arrays.[22] An electronic nose (e-nose) system was reported which used an array of highly sensitive metal-oxide semiconductor (MOS) gas sensors for classification of bacteria into groups. This was based on the class and growth phase of three potentially pathogenic micro-organisms, *E. coli*, *S. aureus* and *Klebsiella oxytoca* (*K. oxytoca*).[23,24] Moreover, a multisensory bacterial volatile compound (BVC) detection system is widely used in the food industry for the detection and monitoring of bacterial contamination.[25] Recent publications have reported the development of e-nose instruments based on measures obtained from multiple sensors in the design of hybrid systems. Examples include MOS sensors combined with GC/MS,[26] metal–organic frameworks combined with MOS sensors,[27] a quartz crystal microbalance (QCM) combined with MOS sensors[28] and a metal oxide semiconductor field effect transistor (MOSFET) combined with MOS sensors.[29] These hybrid gas-sensor array systems have good sensitivity and the ability to detect VOCs and other gases, providing a wide range of possible applications.

Table 1 The normalized concentrations of VOCs from bacteria in culture media

	Gram-negative				Gram-positive
VOC	*E. cloacae*	*E. coli*	*P. aeruginosa*	*S.* Typhi	*S. aureus*
Volatile sulfur compounds (VSCs)					
Dimethyl sulfide, hydrogen sulfide and methyl mercaptan	N/A	6–100[a] (ref. 17 and 18)	17–100[a] (ref. 18)	N/A	59–91[a] (ref. 18)
Aldehydes					
Acetaldehyde, butanal, formaldehyde and 3-methylbutanal	N/A	≈6[a] (ref. 17 and 18)	≈93[a] (ref. 18)	N/A	≈53[a] (ref. 18)
Acids					
Acetic acid and isovaleric acid	N/A	N/A	5–25[b] (ref. 38)	5–25[b] (ref. 38)	≈100[a] (ref. 19), 25–100[b] (ref. 38)
Ketones					
Acetone, 2-cyclopentenone and 2-pentanone	15–20[b] (ref. 20)	≈9[a] (ref. 17)	1–16[b] (ref. 20 and 38)	5–25[b] (ref. 38)	5–25[b] (ref. 38)
Hydrocarbons					
1-Undecene and isoprene	N/A	N/A	≈ 21[a] (ref. 16 and 19), 16–17[b] (ref. 20)	N/A	N/A
Alcohols					
Methanol, ethanol, propanol and 1-butanol	40–100[b] (ref. 20)	1–16[a] (ref. 17, 18 and 39), 5–25[b] (ref. 38)	≈30[a] (ref. 17–19), 25–100[b] (ref. 38)	5–25[b] (ref. 38)	0[a] (ref. 18, 19 and 40), 5–25[b] (ref. 38)
Volatile nitrogen compounds (VNCs)					
Ammonia, acetonitrile, hydrogen cyanide, trimethylamine, indole and 2-aminoacetophenone	N/A	0–6[a] (ref. 18, 40 and 41), 25–100[b] (ref. 38)	0–58[a] (ref. 17–19), 1–25[b] (ref. 38)	1–25[b] (ref. 38)	≈3[a] (ref. 17), 1–5[b] (ref. 38)

[a] Normalization using the min–max normalization $[100 \times ((X_i - X_{Minimum}) \times (X_{Maximum} - X_{Minimum})^{-1})]$, where X is the concentration of VOCs.[42] [b] Normalization using the internal standard (IS) N/A = not available.

There are many kinds of systems that can detect bacterial volatile compounds to a certain extent and do not require Gram staining for identification. But these methods often do not consider the impact of such variables as temperature and stage of the bacterial growth cycle, and so these methods cannot be applied in the medical field as a scanning tool to detect the smell of bacteria growing on or in the body.

At present, there are no reports demonstrating selectivity using organic–inorganic nanocomposite gas sensors coupled with MOS gas sensors in a hybrid e-nose system. Recently, advances have been made with a new method, differential mobility spectrometry (DMS) classification of bacteria.[30]

It successfully classifies all bacterial species and distinguishes Gram status. The publication of this research has yielded many useful rapid bacterial identification technologies, allowing timely initiation of the most appropriate therapy. However, the sensor has limitations in distinguishing bacteria of the same genus. At present, there are no reports demonstrating selectivity using organic–inorganic nanocomposite gas sensors coupled with MOS gas sensors in a hybrid e-nose system. Therefore, our research work will extend the demonstrated functionality of electronic sensing technology beyond the existing landscape. Moreover, our system is aimed at utilizing consumer electronics which are available, affordable and easy-to-use. In this research, we developed a hybrid e-nose system which utilizes two types of gas sensors: (i) three organic–inorganic nanocomposite gas sensors [zinc tetra-*tert*-butyl phthalocyanine (ZnTTBPc), zinc tetra-phenyl porphyrin (ZnTPP), and cobalt tetraphenyl-porphyrin (CoTPP)], coupled with (ii) three MOS gas sensors (TGS 2444, TGS 2603 and TGS 2620). These organic dyes, namely metallo-porphyrin (MP) and metallo-phthalocyanine (MPc), are frequently used as gas sensors based on optical sensing principles because they have delocalized π-systems. These are proven to have high performance as electron transport materials that leads to changes in their optical properties.[31] Recently, organic–inorganic dyes were used as sensor materials forming an integral part of an optical gas sensing system for classification of bacterial species.[32] However, low electrical conductivity of organic–inorganic dyes is an issue in the design and fabrication of electrical gas sensors. The efficiency of electrical conductivity in nanocomposite gas sensors is enhanced by embedding carbon nanotubes (CNTs).[33] In addition, adding CNTs can improve the ability to transfer electrons between the conducting network and VOCs adsorbed onto the sensing surface. The increased aggregate surface area increases the percentage of the sensor response.[32] Thus, nanocomposite gas sensors based on organic–inorganic dyes and carbon nanotubes may detect bacteria and microbial odors in many applications, such as quality control of food products,[34] safety and security,[35] environmental monitoring[36] and medical diagnosis.[37]

The objective of this research was to develop a hybrid e-nose system based on different organic–inorganic materials for bacterial identification. MOS and organic–inorganic based gas sensors were fabricated and installed into the system. This hybrid e-nose system was tested for performance and efficiency on many volatile organic compounds, which represent bacterial volatile compounds such as acetic acid, acetone, ammonia, ethanol, ethyl acetate, formaldehyde and H_2O. In addition, characteristic odors, produced as metabolites of different combinations and quantities of bacteria, were detected and correlated with the Gram stain classification of the bacteria. Five bacterial species, namely *E. coli*, *E. cloacae*, *P. aeruginosa*, *S.* Typhi and *S. aureus*, were distinguished based on their odorants using statistical methods [principal component analysis (PCA) and hierarchical cluster analysis (CA)].

2. Experimental section

2.1. Fabrication of the organic–inorganic dye/multiwall carbon nanotube composite gas sensor

Organic–inorganic dyes, namely zinc-2,9,16,23-tetra-*tert*-butyl-29*H*,31*H*-phthalocyanine (ZnTTBPc), zinc-5,10,15,20-tetraphenyl-21*H*,23*H*-porphyrin (ZnTPP) and cobalt-5,10,15,20-tetraphenyl-21*H*,23*H*-porphine (CoTPP), were purchased from Sigma-Aldrich (St. Louis, MO, USA).

The multiwall carbon nanotubes (MWCNTs) were synthesized using an infusion chemical vapor deposition method from Chiang Mai University.[43] First, ZnTTBPc, ZnTPP and CoTPP were dissolved in a chloroform solution at a concentration of 5 mg ml^{-1} to prepare organic–inorganic dye solutions, while MWCNTs were dispersed in chloroform by means of sonication at a concentration of 2 mg ml^{-1}. Then the MWCNT solution was blended into each organic–inorganic dye solution in order to obtain high electrical conductivity with a ratio of percent loading for the MWCNT solution to dye solution of 50 : 50. Each organic–inorganic dye solution, with MWCNTs dispersed in it, was stirred for 15 min, followed by 30 min of continuous ultrasonic vibration at 25 °C. This was repeated three times to ensure uniformity and homogeneity. [The molecular structures of ZnTTBPc, ZnTPP and CoTPP are shown in Fig. 1(a)]. Finally, three organic–inorganic dye/multiwall carbon nanotube composite mixtures (*i.e.* ZnTTBPc/MWCNT, ZnTPP/MWCNT and CoTPP/MWCNT solutions) were spin-coated onto interdigitated Cr/Au electrodes at 1000 rpm for 30 seconds to produce gas sensor devices, as shown in Fig. 1(b). The interdigitated electrodes (IDEs) were fabricated by E-beam evaporation of Cr/Au thin films deposited on alumina substrates.[44] The thicknesses of the Cr and Au film layers were 50 nm and 200 nm, respectively. The IDEs were an important component of the organic–inorganic dye/MWCNT gas sensor, functioning as the sensing area (the surface area was approximately 0.1×1 mm^2).

2.2. Metal-oxide semiconductor gas sensors

Three commercial metal-oxide semiconductor (MOS) gas sensors, namely TGS 2444, TGS 2603 and TGS 2620, were purchased (Figaro USA Inc., IL, USA). These MOS gas sensors respond to the VOCs in each target gas and other hazardous organic compounds.[45,46] The metal oxide gas sensing materials used with n-type metal oxide semiconductors for bacterial gas sensing are tin oxide (SnO_2)[47] and tungsten trioxide (WO_3).[48] The structures of the single sensing elements are comprised of

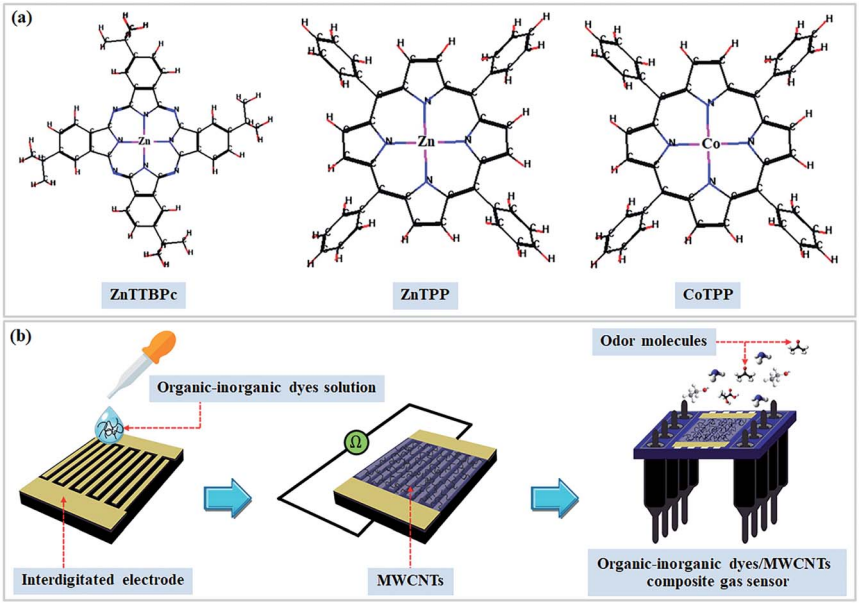

Fig. 1 (a) Structures of ZnTTBPc, ZnTPP and CoTPP, and (b) the fabrication process of the organic–inorganic dye/MWCNT composite gas sensor.

a metal oxide semiconductor layer formed on the alumina substrate of a sensing chip together with an integrated heater. After applying a heating voltage, reducing or oxidizing gases are applied to the sensing layer. The electrical resistance (R) of MOS-type gas sensors changes due to the change in adsorbed oxygen concentration.[48]

2.3. Testing of the hybrid gas sensor arrays

The details of the gas sensor arrays used in our hybrid electronic nose system are listed in Table 2. Organic–inorganic nanocomposite gas sensors can operate in a room-temperature environment, while the MOS gas sensors commonly operate at a high temperature, ranging from 150 °C to 400 °C which requires a heating element. TGS 2444 was highly selective for ammonia gas and had some response to hydrogen sulfide.[45] TGS 2603 was sensitive to low concentrations of the amine-series, air contaminants, and sulfurous vapors, such as trimethyl amine, hydrogen sulfide, hydrogen and ethanol (ethyl alcohol).[46] TGS 2620 was highly selective for general organic solvents such as alcohol, methanol and carbon monoxide.[46] In addition, organic–inorganic dye/multiwall carbon nanotube (MWCNT) composite gas sensors, namely ZnTTBPc/MWCNT, ZnTPP/MWCNT and CoTPP/MWCNT, were used for detection of general organic solvents such as alcohol, acetone, and acetic acid.[32,49]

In this study, the sensitivity and selectivity of gas sensors were tested with acetic acid, acetone, ammonia, ethanol, ethyl acetate, formaldehyde and H_2O. These VOCs have been considered sensitive and specific biomarkers for bacteria. The seven volatile organic compounds were purchased from Merck KGaA (USA), while pure air (zero air) was purchased from Rungcharoen Oxygen Co., Ltd. (Bangkok, Thailand). The details of VOC preparation for testing are shown in Table 3. The number of gas molecules contained in one cubic meter of an ideal gas can be calculated using Loschmidt's number.[50] In addition, the volume of each VOC solution at a concentration of 1000 ppm was calculated based on its molecular weight (MW) and density. A VOC solution was injected into a 1000 ml glass bottle that was placed in a temperature-controlled water bath at the evaporating temperature of that VOC. Each VOC was evaporated at a temperature from 25 °C to 100 °C which was related to its boiling point. Moreover, an zero air carrier system was

Table 2 Details of the gas sensor arrays used in the hybrid electronic nose system

Code	Sensor class	Sensor type (target compounds)	Detection range (ppm)
S1	ZnTTBPc/MWCNT	Nanocomposite gas sensor (organic solvents)	>902[a]
S2	ZnTPP/MWCNT	Nanocomposite gas sensor (organic solvents)	>515[a]
S3	CoTPP/MWCNT	Nanocomposite gas sensor (organic solvents)	>2433[a]
S4	TGS 2444	MOS (ammonia and hydrogen sulfide)	166[a], 10–300[b] (ref. 45)
S5	TGS 2603	MOS (amine-series and sulfurous vapors)	>236[a], 1–10[b] (ref. 46)
S6	TGS 2620	MOS (alcohol and organic solvents)	>141[a], 50–5000[b] (ref. 46)

[a] Typical detection range obtained from the study (see Table 4). [b] Typical detection range was reported by manufacturers of Figaro gas sensors.

Table 3 Preparation of VOCs at a concentration of 1000 ppm in pure air

VOC	Evaporating temperature[a] (°C)	MW (g mol^{-1})	Density (g ml^{-1})	Volume of VOC solution in cylinder (μl)
Acetic acid (35%)	100	60.05	1.05	2.60
Acetone (100%)	56	58.08	0.79	3.29
Ammonia (29%)	25	17.03	0.91	0.84
Ethanol (100%)	78	46.07	0.79	2.62
Ethyl acetate (100%)	77	88.11	0.90	4.38
Formaldehyde (37%)	25	30.03	1.09	1.24
H_2O (100%)	100	18.02	1.00	0.81

[a] Evaporating temperature depends on the boiling point of each VOC.

installed inside the system to spread the VOC's vapor evenly across the bottle and deliver it to the sensor chamber. Then, the resistances of both the sensors were measured; the experiment was repeated three times to obtain a consistent dimension.

2.4. Design of the hybrid electronic nose system

The hybrid electronic nose system was designed in a briefcase form so it could be carried or easily moved. The system consisted of three main components: (i) the gas sensor array unit, (ii) odor-delivery unit, and (iii) data acquisition (DAQ) unit [shown in Fig. 2(a)]. In the gas sensor array unit, there were six different types of gas sensors (Table 2). Three MOS gas sensors and three organic–inorganic dye/MWCNT nanocomposite gas sensors were installed into the sides of the octagon-shaped chamber which was made of Teflon (PTFE) to prevent the VOCs from sticking to the chamber. A schematic of the chamber structure provides two views: the top view and side view [Fig. 2(b)]. The center of the bottom plate of the sensor chamber was pierced to make a gas inlet hole for delivering odors to the electronic nose.

The odor-delivery unit had a solenoid valve for switching between the odor sample (target odor) and zero air (reference gas) for gas delivery into the sensor chamber. Zero air, produced by mixing pure oxygen with pure nitrogen (21% oxygen and 79% nitrogen), was purchased from the gas industry (Rungcharoen Oxygen Co., Ltd., Bangkok). In the olfactory sensitivity testing, zero air (pure air) was used as the carrier gas to deliver the odor sample into the sensor chamber of the hybrid e-nose system. In addition, any background odors contained in the chamber were expelled by zero air flushing. Flow meters were used to monitor the flow rate of the pure air stream in real time so it could be controlled to 400 ml min^{-1}. A data acquisition card (NI USB-6008 of National Instruments, Singapore) with LabVIEW software was installed on a computer and used to convert the analog voltage into a digital signal. Then, the resistance change of each gas sensor was calculated based on a voltage divider concept and sent to the computer.

2.5. Bacterial odor measurement and data processing

Fig. 3 shows a schematic diagram of the hybrid e-nose system for bacterial odor-sensing using two distinct types of gas sensors. In order to test the chemical sensing of the hybrid e-nose, dynamic flow measurements were conducted by switching between the bacteria's odor sample for 2 min and pure air (zero air) for 3 min. This process was repeated for 4 cycles. The temperature was controlled at around 37 °C for bacterial samples and at evaporation temperatures (see in Table 3) for VOC samples. The base-line resistance and the changing

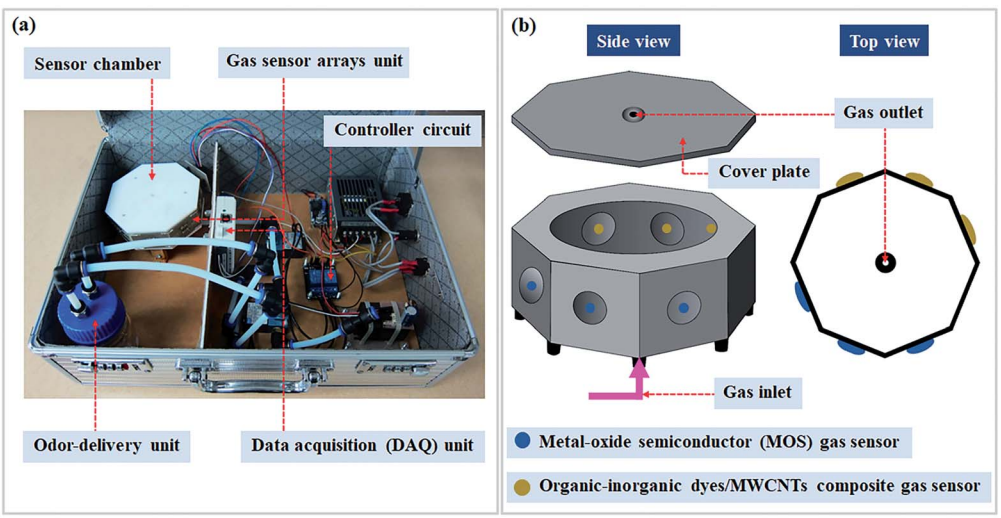

Fig. 2 (a) The physical structure of the hybrid electronic nose system and (b) the schematic of the chamber structure; top view and side view.

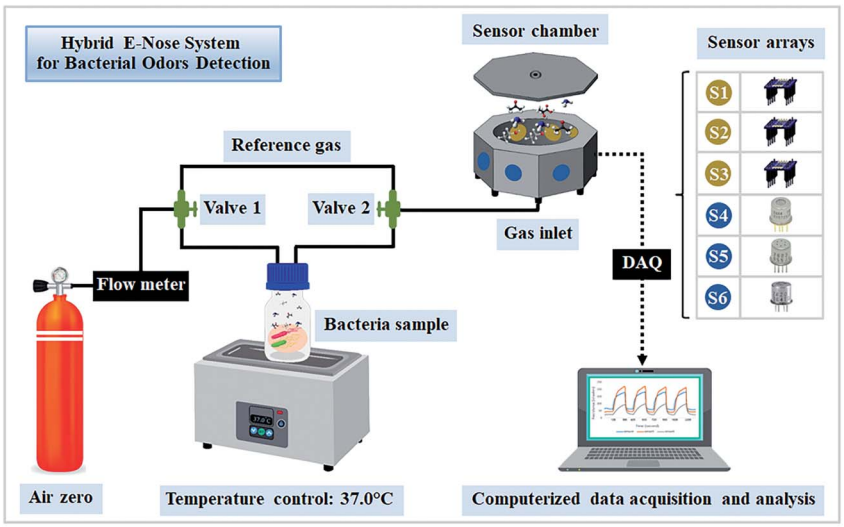

Fig. 3 Schematic diagram of the hybrid e-nose system for detection of bacterial odors.

resistance with time of the gas sensors were recorded every 1 second. The sensor response from each of the six sensors is defined as the difference between the maximum resistance-change (the resistance change upon absorption of the sensed gas) and the baseline resistance (the resistance from zero air). These responses from the sensor arrays were then analyzed based on pattern recognition by principal component analysis, a simple and effective method to recognize patterns in the data by visualizing them in 2-dimensional or 3-dimensional plots.[51] Each experiment was confirmed by analyzing bacterial odor information using a combination of principal component analysis and hierarchical cluster analysis (CA).[52]

The sensor response (S) from each of the six gas sensors was described as the sensitivity of a gas sensor to different gases. Sensitivity (%) was defined by eqn (1) as follows:

$$\text{Sensitivity}\ (\%) = \frac{\Delta R}{R_0} \times 100 \qquad (1)$$

where R_0 is the initial resistance of each sensor without the sample vapor (baseline resistance) and ΔR is the difference in resistance detected by the sensor between the bacterial odor and pure air.

2.6. Bacterial sample preparation

The five bacterial pathogens investigated in this study were *Enterobacter cloacae* subsp. *cloacae* (ATCC 13047), *Staphylococcus aureus* subsp. *aureus* (ATCC 29213), *Escherichia coli* (ATCC 25244), *Pseudomonas aeruginosa* (ATCC 27853) and *Salmonella enterica* subsp. *enterica serovar* Typhi or *S.* Typhi (ATCC 19430). Each of these selected bacteria can cause nosocomial infection, some are found in the natural environment, and all tend to be resistant to disinfectants and antibiotics. The strains were obtained from the Faculty of Medical Technology, Mahidol University, Thailand. Briefly, the bacteria were grown in sterile nutrient media at 37 °C for cell recovery and then single isolated colonies were sub-cultured in Luria–Bertani (LB) liquid medium at 37 °C in a shaking incubator (180 rpm) for 9 h. Cloudy media after cultivation were observed and measured for bacterial growth characteristics. The initial concentration of bacteria was determined using optical density (at 600 nm). Bacterial growth cultures were optimized and adjusted until an OD600 of 0.3 was reached. Then, a batch culture was prepared by transferring 25 μl of each bacterial culture into 25 ml of LB broth to control the initial bacterial number in the sample bottles for odor detection.

These bacterial cultures were then grown at a constant incubation temperature (IT) of 37 °C. Culture samples were removed at intervals and the number of viable bacteria was counted *via* the increasing turbidity as observed at OD600. A logarithmic growth curve for each bacterial strain was plotted. Finally, the OD600 value and gas sensing response to each bacterial culture were collected every 3 hours.

3. Results and discussion

3.1. Bacterial growth curve analysis

The growth phase of five bacterial species in liquid culture media was measured using the optical density at 600 nm (OD600) of the culture suspensions with a UV-visible spectrophotometer. The initial cell concentration of the five bacterial species was standardized by using the same value of optical density (OD600 nm). The growth curve of the bacteria was plotted by measuring OD600 values from 0 to 12 h incubation (Fig. 4).

Growth curves were obtained using the polynomial regression equation, *i.e.* $Y = A_1 + (A_2 + A_1)(1 + 10^{[(\log X_0 - X) \times P]})$, where X is time, Y is optical density and A_1, A_2, and P are constant values. The cell density of all cultures increased slightly during the first 2 h of incubation and then rapidly during hours 3–8. The stationary phases (no further increase in cell density) of the five bacterial species were observed after 9 h of incubation. There was a different logarithm of living bacterial cells for each of the

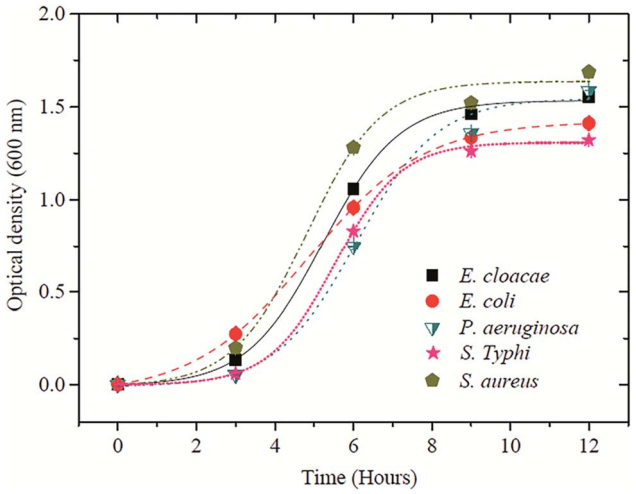

Fig. 4 The optical densities of *E. cloacae*, *E. coli*, *P. aeruginosa*, *S. aureus* and *S.* Typhi in liquid culture media were obtained in triplicate samples.

five pathogens, and each had a high R-squared (R^2) value. At the exponential (log) phase (6 h incubation), *S. aureus* had the greatest cell density when compared with those of *E. cloacae*, *E. coli*, *S.* Typhi and *P. aeruginosa* (the coefficient of determination; R^2 values of 0.99415, 0.99857, 0.99998, 0.99929 and 0.99003, respectively). A typical four-phase pattern of bacterial growth was seen in this study for each species. However, *S. aureus* and *E. cloacae* entered log phase growth quicker than *E. coli*, *S.* Typhi and *P. aeruginosa* which each displayed a prolonged lag period.[20] The unique growth behaviors of different pathogens might have been related to species-specific odor-releasing processes.

3.2. Sensor performance and calibration at elevated VOC concentrations

In order to evaluate the performance of the self-built hybrid e-nose system for bacterial identification, seven volatile organic compounds (VOCs), produced by bacteria as waste products, were selected to further evaluate the sensor performance based on sensitivity and specificity. Specifically, acetic acid, acetone, ammonia, ethanol, ethyl acetate, formaldehyde and H_2O at a concentration of 1000 ppm were utilized in the assessment.

In analytical chemistry, researchers calculate the limit of detection (LOD)[53]: the smallest amount or concentration of an analyte gas in the test sample that can be reliably distinguished from pure air or the blank. The LODs of seven VOCs with six different gas sensors are presented in Table 4. The LOD is defined according to eqn (2) as follows:

$$\mathrm{LOD} = 3 \times \frac{\mathrm{SD_{blank}}}{\mathrm{slope}} \quad (2)$$

where SD_{blank} is the standard deviation of the blank signal (or sensor signal under pure air flow) and *slope* is the slope of the sensitivity curve which is measured in the concentration range of 1000–3000 ppm. The concentration of each VOC was measured three times to check reproducibility.

Choosing the most appropriate gas sensors for detection of each bacterial odor used volatile testing in the dynamic system in order to achieve optimal detection and sensitivity of each sensor. It was found that six hybrid gas sensor arrays, three organic–inorganic nanocomposite gas sensors (ZnTTBPc, ZnTPP and CoTPP) coupled with three commercial metal-oxide semiconductor (MOS) gas sensors (TGS 2444, TGS 2603 and TGS 2620), under dynamic gas flow testing showed excellent sensitivity (Fig. 5). The sensitivity for the three organic–inorganic nanocomposite gas sensors was expected to be in the range of approximately 0.002% to 1.41% at 1000 ppm. The three commercial MOS gas sensors had a wide sensitivity range (from 1.86% to 99.03%) as well as a quick response and short recovery time. The MOS gas sensors provided greater sensitivity than the organic–inorganic nanocomposite gas sensors. However, each sensor showed a significantly different pattern of specific volatile organic compounds.

Among the organic–inorganic nanocomposite gas sensors, the CoTPP/MWCNT gas sensor (S3) showed the highest sensitivity to ethyl acetate, which is found in volatile bacterial metabolites.[54] The ZnTPP/MWCNT gas sensor (S2) demonstrated a striking response when detecting acetic acid, mainly related to the growth of *P. aeruginosa*, *S.* Typhi and *S. aureus*.[19,38] Moreover, the bar chart (Fig. 5) also shows that water elicited negligible responses from all sensors and so should not have any significant influence on the accuracy of the analytical results.[55] Therefore, we conclude that these sensors, fabricated from porphyrin and phthalocyanine, are well suited for use as sensor arrays for volatile biomarkers in bacterial odors. Among the MOS gas sensors, the TGS 2603 gas sensor (S5) yielded its highest response to acetic acid, and then, in decreasing order, to formaldehyde, ethanol and acetone. The TGS 2620 gas sensor (S6) showed the second highest responses to acetic acid, ethanol and acetone. In contrast, the TGS 2444 gas sensor (S4) showed similar minor responses to all seven VOCs tested. However, inclusion of the full set of sensors (S1–S6) in this hybrid e-nose system was necessary to generate the odor-specific patterns which detected and identified the bacteria-specific odors. Study of the practical considerations in gas sensor performance not only demonstrates excellent sensitivity and outstanding selectivity to the target gas molecules, but also the stability after being used for a long time. Long-term stability experiments were conducted on six gas sensors toward pure air (without gas) over a total period of 30 days, as shown in Fig. 6. The standard deviation (SD) of baseline resistance for each of

Table 4 Limit of detection (LOD) of gas sensor arrays for seven VOCs (ppm)

VOCs	S1	S2	S3	S4	S5	S6
Acetic acid	902	578	5713	369	329	174
Acetone	3282	1233	9380	466	1502	339
Ammonia	4108	1041	6075	166	441	152
Ethanol	1297	7362	5786	755	3782	141
Ethyl acetate	1554	515	2433	490	236	164
Formaldehyde	1341	840	10 194	2143	1444	219
H_2O	105 138	96 284	243 550	583	2225	345

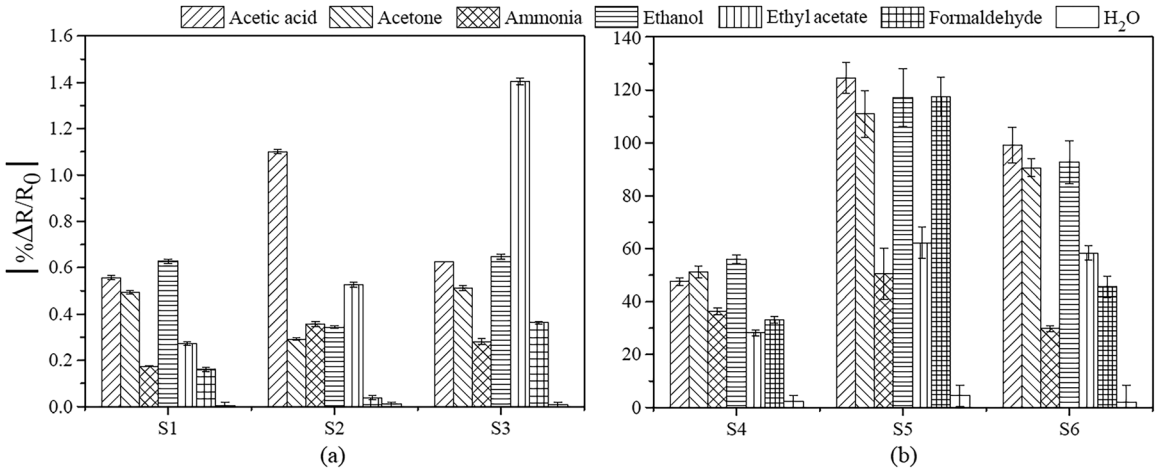

Fig. 5 Average sensitivity (%) for (a) organic–inorganic nanocomposite gas sensors and (b) commercial metal-oxide semiconductor (MOS) gas sensors toward seven VOCs at a concentration of 1000 ppm under dynamic gas flow testing (400 ml min^{-1}).

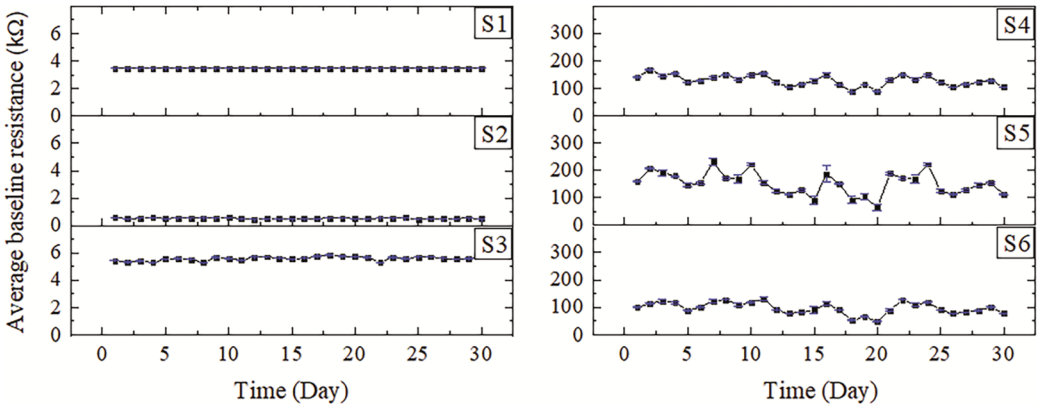

Fig. 6 The relationship between the long-term stability of the baseline resistance and the aging time for three organic–inorganic nanocomposite gas sensors (S1–S3) and three commercial metal-oxide semiconductor (MOS) gas sensors (S4–S6).

the six gas sensors (S1–S6) was 0.05, 6.16, 2.60, 14.98, 27.05 and 22.28%, respectively. It is clearly shown that the SDs of the baseline resistance for the three organic–inorganic nanocomposite gas sensors (S1–S3) were each less than 10% toward pure air, which revealed the great stability of the sensors, while the SDs of the three commercial metal-oxide semiconductor (MOS) gas sensors (S4–S6) were each more than 10% toward pure air, which revealed their poor stability.

3.3. Detection and analysis of bacterial volatile organic compounds

Fig. 7 shows the sensing signals on an organic–inorganic nanocomposite gas sensor (CoTPP/MWCNT; S3) and a commercial metal-oxide semiconductor gas sensor (TGS 2620; S6) recorded as changes in resistance as a function of time of the five types of bacterial odors at 6 h incubation. The dynamic flow measuring was performed by switching between the baseline detection of pure air (zero air) for 3 min and the detection of the sample bacteria's odor for 2 min. This cycle was repeated four times.

After three seconds, we observed an abrupt change in the resistance values of the CoTPP/MWCNT gas sensor (S3) when exposed to each bacterial volatile compound [Fig. 7(a)]. In contrast, for the same samples the resistance values of the TGS 2620 gas sensor (S6) decreased abruptly to reach its lower resistance [Fig. 7(b)]. These results showed that the organic–inorganic nanocomposite gas sensors (S1–S3) were n-type semiconductors, whereas the MOS gas sensors were p-type semiconductors, increasing and decreasing the resistivity under oxidizing gas conditions.[56] The resistance changes during gas sensing of the two types of gas sensors were different, in accordance with their distinct sensing mechanisms. The differences between the signals from the bacterial odor and pure air (base line) were used as features in the PCA and CA analyses.[51,52]

The ZnTPP/MWCNT (S2) and TGS 2603 (S5) gas sensors were specifically required for detection of acetic acid vapor. This vapor was found at high levels from Gram-positive bacteria (*S. aureus*) but was not found in vapors of two of the Gram-negative bacteria (*E. coli* and *E. cloacae*) (see Table 1). These sensors have

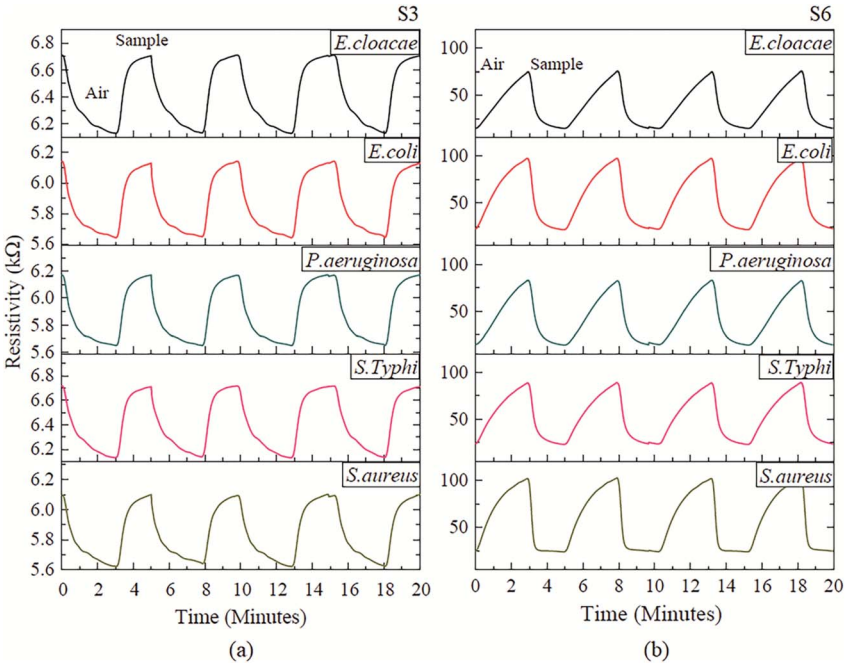

Fig. 7 The sensing signals of the (a) CoTPP/MWCNT gas sensor (S3) and (b) TGS 2620 gas sensor (S6) in response to five types of bacterial odors after 6 h incubation as measured using the self-built hybrid electronic nose.

also been tested with other volatile biomarkers (ammonia, ethyl acetate and water) and were found to have less sensitivity for them.

The graphs in Fig. 5 and 8 show the sensitivities of each sensor (S1–S6) when tested for seven volatile compounds in five bacterial odor samples. It was found that the TGS 2603 (S5) and TGS 2620 (S6) gas sensors were the most sensitive for detecting *E. cloacae* odor. These results were consistent with the amounts of acetic acid, formaldehyde, ethanol, acetone and ethyl acetate forming the volatile constituents of each bacterial odor. In addition, the CoTPP/MWCNT (S3) and ZnTPP/MWCNT (S2) gas sensors demonstrated striking responses when detecting *E. cloacae* and *P. aeruginosa*, respectively.

The *p*-value approach to hypothesis testing with a significance level of 95% was used to compare the sensitivity of each sensor to each bacterial odor from four Gram-negative and one Gram-positive bacterial sample released after 6 h of incubation at 37 °C. Their statistical significances (*p*-value in parentheses) were S1 (0.03), S2 (0.01), S3 (0.00), S4 (0.01), S5 (0.30) and S6 (0.03). This revealed that the TGS 2603 gas sensor (S5) showed no statistically significant difference in its sensitivity to Gram-negative and Gram-positive bacteria. However, the sensitivities

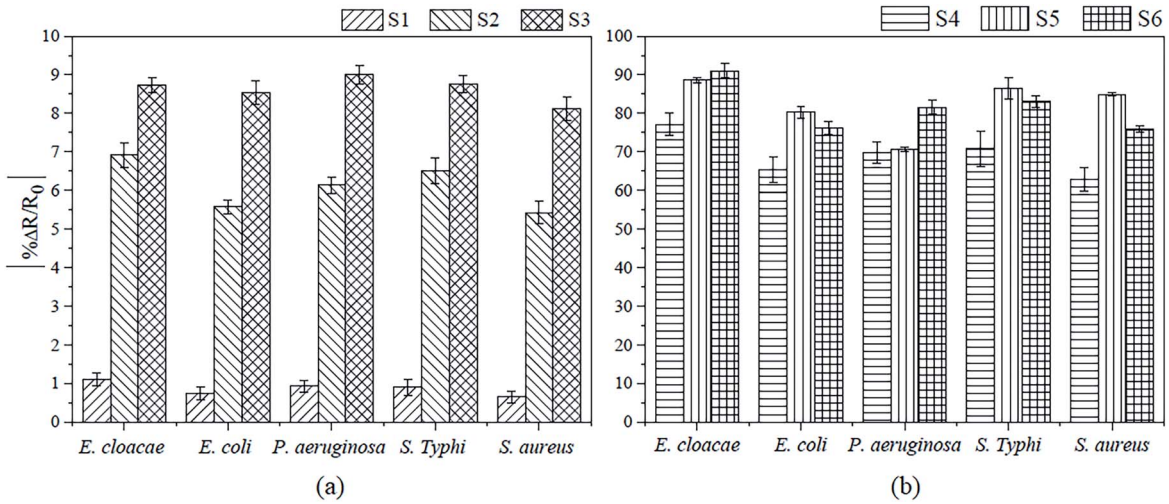

Fig. 8 The sensitivity of the organic–inorganic nanocomposite gas sensors (S1–S3) and the commercial metal-oxide semiconductor gas sensors (S4–S6) obtained upon exposure to volatile biomarkers from five different species of bacteria at an incubation period of 6 h at 37 °C.

of the other five sensors (S1, S2, S3, S4 and S6) were significantly different based on the Gram staining results.

The effect of incubation duration on the bacterial growth and metabolic activity of the five species of pathogenic bacteria, and their yield of volatile biomarkers allowing species discrimination, was investigated through sniffing every 3 h. Principal component discrimination analysis score plots were created in order to find odor patterns which enhanced discrimination. The odors produced by the five species of bacteria (*E. cloacae*, *E. coli*, *P. aeruginosa*, *S.* Typhi and *S. aureus*) and culture media after different lengths of incubation were distinguished and grouped using ellipses based on 95% confidence.[57] The odor patterns shown in Fig. 9(a) and (d) show that the clusters of the five species of bacteria and culture media during the lag (3 h) and stationary (12 h) phases were not clearly separated. This implies that each bacterial sample's odor during these incubation phases had few differences.

Discrimination of odor components was seen at 6 h of incubation of *E. cloacae*, *E. coli*, *P. aeruginosa*, *S.* Typhi and *S. aureus* and culture media (Fig. 9(b)). PC1 and PC2 account for 92.40% and 7.20% of the variance, respectively, which completely separated the odor data of each bacterial species and culture media. Therefore, it seems certain that the results of bacterial odor discrimination were not influenced by culture media odor. The growth curves (see Fig. 4) showed that the 6 h time points occurred during the log phase of the bacterial growth cycles, the time when the cells were dividing and doubling in number. This is the phase when metabolic activity is high, and DNA, RNA, cell wall components, and other substances necessary for growth are generated to support division.[41,58] Therefore, the hybrid e-nose had the ability to identify unique odor patterns associated with each bacterial species when their metabolism made these prominent and thus useful for further diagnostic applications.

Although the bacterial odors from the five species at 9 h of incubation (shown in Fig. 9(c)) were separated into five groups on the PCA plots, they stood quite close to each other on the PCA axis and overlapped with the culture media. PC1 and PC2 contributed 91.9% and 7.6% of the total variance, respectively. As a matter of fact, in the stationary phase the number of dividing cells equals the number of dying cells[59] and results in no overall population growth. The cells become less metabolically active and less volatile biomarkers are released from cultures.[41]

Gram staining helps to differentiate bacterial species, allowing the diagnosis of infections and identification of which species gives a food it's fantastic character. Gram staining is a common technique used to differentiate two large groups of bacteria based on the structure of their cell walls.[60] The two key features that lead to the differentiation of Gram-positive and

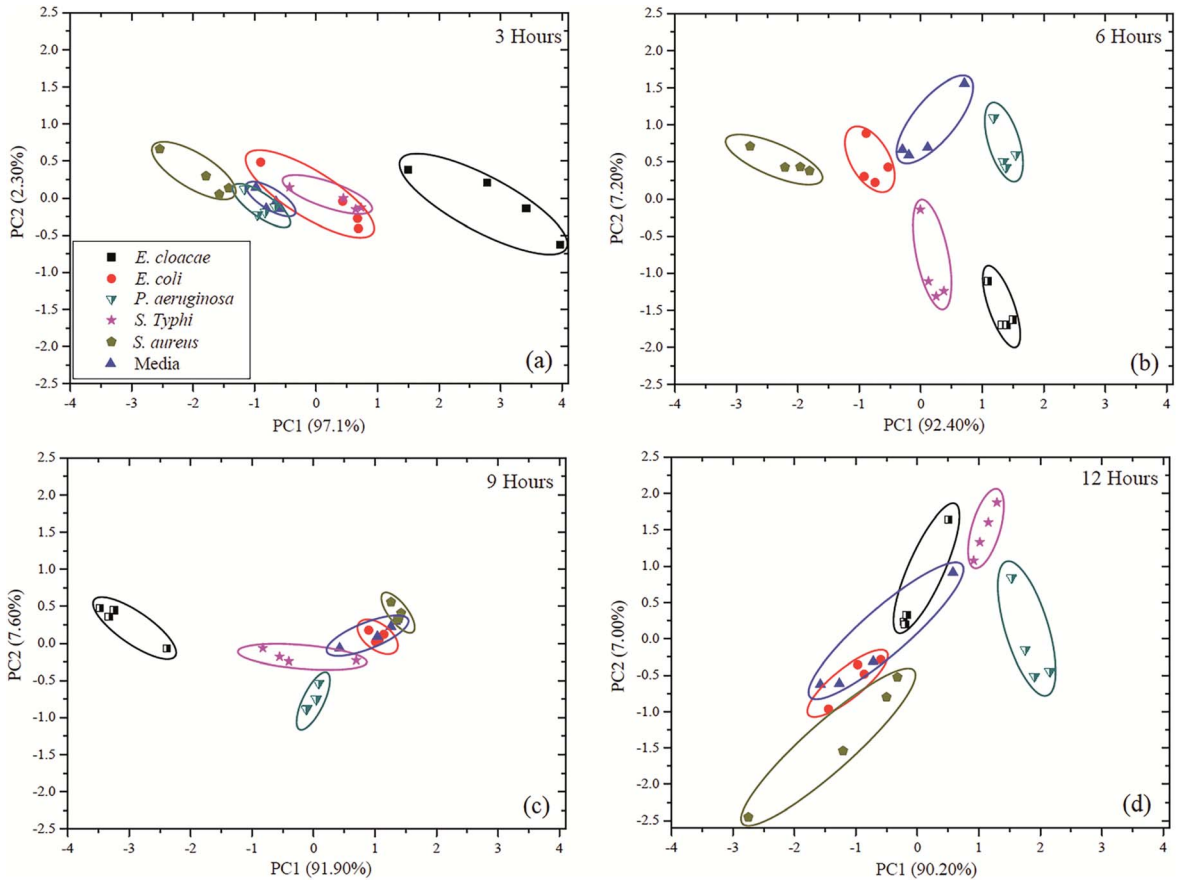

Fig. 9 Schematic diagrams of principal component analysis (PCA) of culture media and five species of pathogenic bacteria in culture media with self-built hybrid e-nose measurements at (a) 3 h, (b) 6 h, (c) 9 h and (d) 12 h incubation times.

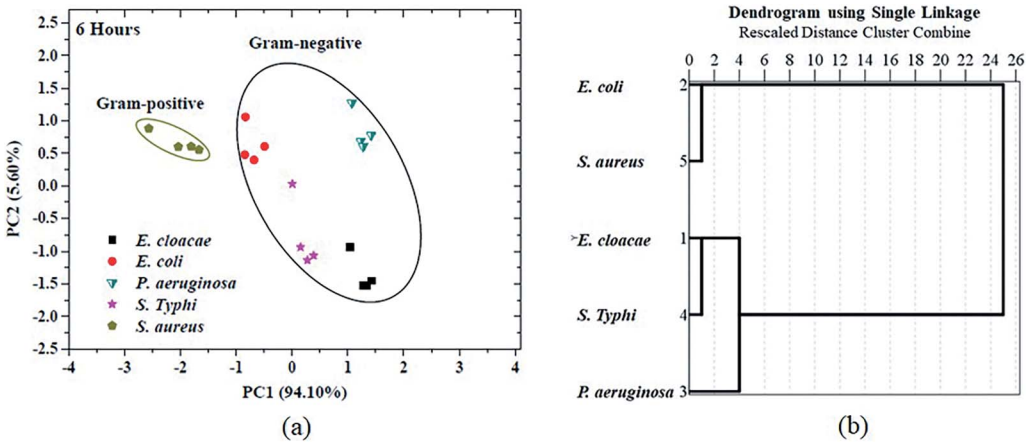

Fig. 10 (a) 2D principal component analysis (PCA) and (b) cluster analysis (CA) performed on bacteria odor data between the Gram-negative group and Gram-positive group.

Gram-negative species are the thickness of the peptidoglycan layer and the presence or absence of an outer lipid membrane.[61] Though both groups of bacteria can cause diseases, their respective treatments differ. For bacterial infections, Gram staining helps determine what kind of medication is needed for the best results. In this research, discrimination between Gram-positive and Gram-negative bacteria may be performed accurately by using the e-nose. Volatile compounds of four Gram-negative and one Gram-positive bacterial species, after 6 h of incubation, were identified and clustered separately using pattern recognition methods based on principal component analysis and hierarchical cluster analysis (Fig. 10).

The results of PCA and CA analyses [shown in Fig. 10(a) and (b)] revealed that the bacterial odor patterns from the group of Gram-negative bacteria (black ellipse) were clearly separated from those of the Gram-positive species (green ellipse), $p < 0.05$. Furthermore, this suggested that some volatile constituents in the bacterial odor of each species were obviously different. The interpretation of the results of CA was that bacterial odor data formed two major groups: odors from *E. cloacae*, *E. coli*, *P. aeruginosa* and *S.* Typhi (all Gram-negative bacteria) and from *S. aureus* (a Gram-positive bacterium). The maximum distance between the two comparative bacterial groups was significantly different.[25] Intra-group similarity was demonstrated as two bacterial odor samples from the Gram-negative group (*E. cloacae* and *P. aeruginosa*) showed a single-linkage (nearest neighbor) distance of close to 4. The minimum distance between *E. cloacae* and *S.* Typhi was approximately 1, which was at an equal distance between *E. coli* and *S. aureus*. Therefore, while the Gram-negative bacterial odors were all different from each other, they were each distinct from the Gram-positive bacterial odor. This was confirmed by analyzing bacterial odor information by a combination of principal component and hierarchical cluster analyses.

4. Conclusions

A self-built hybrid electronic nose prototype which combined three organic–inorganic nanocomposite gas sensors and three commercial metal-oxide semiconductor gas sensors was developed. The three nanocomposite gas sensors were successfully fabricated from a combination of carbon nanotube and organic–inorganic dyes, *i.e.* ZnTTBPc, ZnTPP and CoTPP. The gas sensor arrays provided an acceptable limit of detection and sensitivity when assaying seven volatile organic compounds released from bacterial cultures. Combined with PCA analysis, the hybrid electronic nose discriminated the odors from *E. cloacae*, *E. coli*, *P. aeruginosa*, *S.* Typhi and *S. aureus* (after 6 h of incubation) with 99.7% of the total variance. Based on the CA analysis, four Gram-negative bacteria (*i.e.*, *E. cloacae*, *E. coli*, *P. aeruginosa* and *S.* Typhi) were completely separated from one Gram-positive bacteria (*S. aureus*) with an approximate distance of 25. According to the results, we conclude that this hybrid electronic nose prototype has high potential to identify bacterial species as a non-invasive, pathogenic bacterial monitoring system and has several advantages such as being easy to use, cost effective, rapid and non-destructive.

Conflicts of interest

There are no conflicts to declare.

Acknowledgements

This project was supported by Mahidol University and the Thailand Research Fund (TRF) (Grant No. MRG6080151).

References

1 R. T. Noble and S. B. Weisberg, *J. Water and Health*, 2005, **3**, 381–392.
2 A. Y. Katukiza, M. Ronteltap, P. van der Steen, J. W. A. Foppen and P. N. L. Lens, *J. Applied Microbiology*, 2014, **116**, 447–463.
3 N. Massad-Ivanir, G. Shtenberg, N. Raz, C. Gazenbeek, D. Budding, M. P. Bos and E. Segal, *Sci. Rep.*, 2016, **6**, 38099.
4 N. T. Thet and A. T. A. Jenkins, *Electrochem. Commun.*, 2015, **59**, 104–108.

5 Y. Chen, N. Cheng, Y. Xu, K. Huang, Y. Luo and W. Xu, *Biosens. Bioelectron.*, 2016, **81**, 317–323.
6 K. Rijal and R. Mutharasan, *Analyst*, 2013, **138**, 2943–2950.
7 I. Musil, V. Jensen, J. Schilling, B. Ashdown and T. Kent, *J. Med. Case Rep.*, 2010, **4**, 131.
8 Y. Xu, W. Cheung, C. L. Winder and R. Goodacre, *Anal. Bioanal. Chem.*, 2010, **397**, 2439–2449.
9 L. Váradi, J. L. Luo, D. E. Hibbs, J. D. Perry, R. J. Anderson, S. Orenga and P. W. Groundwater, *Chem. Soc. Rev.*, 2017, **46**, 4818–4832.
10 P. Mazoteras, P. J. M. Bispo, A. L. Höfling-Lima and R. P. Casaroli-Marano, *Curr. Eye Res.*, 2015, **40**, 697–706.
11 R. M. Hagen, H. Frickmann, M. Elschner, F. Melzer, H. Neubauer, Y. P. Gauthier, P. Racz and S. Poppert, *Int. J. Med. Microbiol.*, 2011, **301**, 585–590.
12 H. M. Al-Qadiri, M. A. Al-Holy, M. Lin, N. I. Alami, A. G. Cavinato and B. A. Rasco, *J. Agric. Food Chem.*, 2006, **54**, 5749–5754.
13 X. Yu, W. Jiang, Y. Shi, H. Ye and J. Lin, *J. Cell Mol. Med.*, 2019, **23**, 7143–7150.
14 N. Singhal, M. Kumar, P. K. Kanaujia and J. S. Virdi, *Front. Microbiol.*, 2015, **6**, 791.
15 E. Tait, J. D. Perry, S. P. Stanforth and J. R. Dean, *Trac. Trends Anal. Chem.*, 2014, **53**, 117–125.
16 A. W. Boots, A. Smolinska, J. J. B. N. Van Berkel, R. R. R. Fijten, E. E. Stobberingh, M. L. L. Boumans, E. J. Moonen, E. F. M. Wouters, J. W. Dallinga and F. J. Van Schooten, *J. Breath Res.*, 2014, **8**, 027106.
17 M. K. Storer, K. Hibbard-Melles, B. Davis and J. Scotter, *J. Microbiol. Methods*, 2011, **87**, 111–113.
18 R. M. S. Thorn, D. M. Reynolds and J. Greenman, *J. Microbiol. Methods*, 2011, **84**, 258–264.
19 W. Filipiak, A. Sponring, M. M. Baur, A. Filipiak, C. Ager, H. Wiesenhofer, M. Nagl, J. Troppmair and A. Amann, *BMC Microbiol.*, 2012, **12**, 113.
20 O. Lawal, H. Knobel, H. Weda, T. M. E. Nijsen, R. Goodacre, S. J. Fowler, W. M. Ahmed, A. Artigas, J. Bannard-Smith, L. D. J. Bos, M. Camprubi, L. Coelho, P. Dark, A. Davie, E. Diaz, G. Goma, T. Felton, S. J. Fowler, J. H. Leopold, P. M. P. van Oort, P. Povoa, C. Portsmouth, N. J. W. Rattray, G. Rijnders, M. J. Schultz, R. Steenwelle, P. J. Sterk, J. Valles, F. Verhoeckx, A. Vink, I. R. White, T. Winters and T. Zakharkina, *Metabolomics*, 2018, **14**, 66.
21 R. Rocchi, M. Mascini, A. Faberi, M. Sergi, D. Compagnone, V. Di Martino, S. Carradori and P. Pittia, *Food Contr.*, 2019, **106**, 106736.
22 T. Seesaard, P. Lorwongtragool and T. Kerdcharoen, *Sensors*, 2015, **15**, 1885–1902.
23 J. W. Gardner, M. Craven, C. Dow and E. L. Hines, *Meas. Sci. Technol.*, 1998, **9**, 120–127.
24 J. Carrillo and C. Durán, *Biosensors*, 2019, **9**, 23.
25 V. Sberveglieri, E. N. Carmona, E. Comini, A. Ponzoni, D. Zappa, O. Pirrotta and A. Pulvirenti, *BioMed Res. Int.*, 2014, **2014**, 1–6.
26 O. Gould, T. Wieczorek, B. De Lacy Costello, R. Persad and N. Ratcliffe, *J. Breath Res.*, 2018, **12**, 1.
27 X. Wu, S. Xiong, Y. Gong, Y. Gong, W. Wu, Z. Mao, Q. Liu, S. Hu and X. Long, *Sensor. Actuator. B Chem.*, 2019, **292**, 32–39.
28 Ü Özsandıkcıoğlu, A. Atasoy and Ş Yapıcı, *2018 IEEE International Symposium on Medical Measurements and Applications (MeMeA)*, 2018.
29 J.-E. Haugen and I. Undeland, *J. Agric. Food Chem.*, 2003, **51**, 752–759.
30 L. Hokkinen, A. Kesti, J. Lepomäki, O. Anttalainen, A. Kontunen, M. Karjalainen, J. Aittoniemi, R. Vuento, T. Lehtimäki, N. Oksala and A. Roine, *Future Microbiol.*, 2020, **15**, 233–240.
31 D. M. Guldi and S. Fukuzumi, *J. Porphyr. Phthalocyanines*, 2002, **6**, 289–295.
32 S. Kladsomboon, C. Thippakorn and T. Seesaard, *Sensors*, 2018, **18**, 3189.
33 T. Sarkar, S. Srinives, S. Sarkar, R. C. Haddon and A. Mulchandani, *J. Phys. Chem. C*, 2014, **118**, 1602–1610.
34 S. Cui, L. Yang, J. Wang and X. Wang, *Sensor. Actuator. B Chem.*, 2016, **233**, 337–346.
35 T. Seesaard, S. Seaon, C. Khunarak, P. Lorwongtragool and T. Kerdcharoen, *11th International Conference on Electrical Engineering/Electronics*, Computer, Telecommunications and Information Technology, 2014.
36 A. Kaushik, R. Kumar, S. K. Arya, M. Nair, B. D. Malhotra and S. Bhansali, *Chem. Rev.*, 2015, **115**, 4571–4606.
37 T. Eamsa-ard, T. Seesaard, T. Kitiyakara and T. Kerdcharoen, *9th Biomedical Engineering International Conference (BMEiCON)*, 2016.
38 J. Zhu, H. D. Bean, Y.-M. Kuo and J. E. Hill, *J. Clin. Microbiol.*, 2010, **48**, 4426–4431.
39 L. D. J. Bos, P. J. Sterk and M. J. Schultz, *PLoS Pathog.*, 2013, **9**(5), 1–8.
40 M. Jünger, W. Vautz, M. Kuhns, L. Hofmann, S. Ulbricht, J. I. Baumbach, M. Quintel and T. Perl, *Appl. Microbiol. Biotechnol.*, 2012, **93**, 2603–2614.
41 C. Zscheppank, H. L. Wiegand, C. Lenzen, J. Wingender and U. Telgheder, *Anal. Bioanal. Chem.*, 2014, **406**, 6617–6628.
42 K. Y. Jain and K. S. Bhandare, *Int. J. Electron. Commun. Comput. Technol.*, 2014, **3**, 45–50.
43 P. Singjai, S. Changsarn and S. Thongtem, *Mater. Sci. Eng., A*, 2007, **443**, 42–46.
44 P. Lorwongtragool, A. Wisitsoraat and T. Kerdcharoen, *J. Nanosci. Nanotechnol.*, 2011, **11**, 10454–10459.
45 T. Jayasree, M. Bobby and S. Muttan, *J. Med. Biol. Eng.*, 2015, **35**, 759–764.
46 R. Rusinek, M. Gancarz and A. Nawrocka, *LWT*, 2020, **117**, 108665.
47 A. Šetkus, A.-J. Galdikas, Ž.-A. Kancleris, A. Olekas, D. Senulienė, V. Strazdienė, R. Rimdeika and R. Bagdonas, *Sensor. Actuator. B Chem.*, 2006, **115**, 412–420.
48 Y. Zhu, Y. Zhao, J. Ma, X. Cheng, J. Xie, P. Xu, H. Liu, H. Liu, H. Zhang, M. Wu, A. A. Elzatahry, A. Alghamdi, Y. Deng and D. Zhao, *J. Am. Chem. Soc.*, 2017, **139**, 10365–10373.
49 S. Kladsomboon, M. Lutz, T. Pogfay, T. Puntheeranurak and T. Kerdcharoen, *J. Nanosci. Nanotechnol.*, 2012, **12**, 5240–5244.

50 M. E. Zhussupov, *International Journal of Fundamental Physical Sciences*, 2014, **4**, 62–71.
51 H. M. Jeon, J. Y. Lee, G. M. Jeong and S. I. Choi, *PloS One*, 2018, **13**(7), 1–9.
52 H. Fan, V. H. Bennetts, E. Schaffernicht and A. J. Lilienthal, *Sensor. Actuator. B Chem.*, 2018, **259**, 183–203.
53 E. Desimoni and B. Brunetti, *Pharm. Anal. Acta*, 2015, **6**, 355.
54 K. A. Hettinga, H. J. F. Van Valenberg, T. J. G. M. Lam and A. C. M. Van Hooijdonk, *J. Dairy Sci.*, 2008, **91**, 3834–3839.
55 H. T. Ngo, K. Minami, G. Imamura, K. Shiba and G. Yoshikawa, *Sensors*, 2018, **18**(5), 1–11.
56 A. Dey, *Mater. Sci. Eng. B*, 2018, **229**, 206–217.
57 K. Timsorn, T. Thoopboochagorn, N. Lertwattanasakul and C. Wongchoosuk, *Biosyst. Eng.*, 2016, **151**, 116–125.
58 K. Wiesner, M. Jaremek, R. Pohle, O. Von Sicard and E. Stuetz, *Procedia Eng.*, 2014, **87**, 332–335.
59 P. Pletnev, I. Osterman, P. Sergiev, A. Bogdanov and O. Dontsova, *Acta Naturae*, 2015, **7**, 22–33.
60 S. C. Becerra, D. C. Roy, C. J. Sanchez, R. J. Christy and D. M. Burmeister, *BMC Research Notes*, 2016, **9**, 216.
61 T. J. Silhavy, D. Kahne and S. Walker, *Cold Spring Harbor Perspect. Biol.*, 2010, **2**, a000414.